Proceedings of the Canadian Society for Mechanical Engineering International Congress
32nd Annual Conference of the Computational Fluid Dynamics Society of Canada
Canadian Society of Rheology Symposium
CSME-CFDSC-CSR 2025
May 25–28, 2025, Montréal, Québec, Canada

Incorporating Copper Wire Mesh Into a PCM-Based Battery Pack

Mohammmad J. Ganji[1*], Martin Agelin-Chaab[1], Marc A. Rosen[1]
[1]Faculty of Engineering and Applied Science, Ontario Tech University, Oshawa, Canada
*mohammadjavad.ganji@ontariotechu.ca

Abstract

Effective thermal management is essential for maintaining the performance and lifespan of lithium-ion batteries. This study introduces an innovative approach by incorporating a partial copper wire mesh within a PCM-based battery pack to enhance heat dissipation. Nine series-connected 21700 lithium-ion cells (5000 mAh) were subjected to constant discharge rates of 1C to 3C (5A to 15A) at an ambient temperature of 22 °C. A thermodynamic energy balance framework was employed to quantify heat generation, dissipation, and latent heat utilization. Experimental results indicate that integrating the copper mesh significantly improved heat dissipation, lowered peak cell temperatures, and reduced dependence on the PCM's latent heat capacity. Compared to the conventional PCM-only system, the mesh-PCM configuration decreased maximum temperatures by 3.7, 2.6, and 4.8 °C at 1C, 2C, and 3C discharge rates, respectively, while increasing heat dissipation by 20-40%. At moderate discharge rates (1C and 2C), the mesh-PCM system effectively managed heat without requiring latent heat utilization, while at 3C, the PCM melting fraction was reduced from 15.3% to 9.9%. This demonstrates the stable thermal conditions and extends safe operational limits up to 3C (15A). These findings highlight the potential of copper mesh integration to enhance the efficiency of PCM-based BTMS, offering a lightweight and effective alternative to conventional cooling methods. Future work should focus on optimizing mesh design parameters to further improve thermal regulation and sustain reliability under higher discharge rates.

Keywords: Battery Thermal Management System, Phase Change Material, Copper Wire Mesh, Experimental Analysis, Li-ion cylindrical cells.

I. INTRODUCTION

Lithium-ion batteries (LIBs) have emerged as the dominant energy storage technology for electric and hybrid vehicles due to their high specific energy, long cycle life, and low self-discharge rates [1]. These attributes make LIBs ideal for applications demanding high energy density and reliability. However, the thermal management of LIBs remains a critical challenge, particularly under high discharge rates. The heat generated during charging and discharging can lead to safety concerns and reduced operational efficiency. Excessive temperatures degrade the battery's capacity and pose risks of thermal runaway and fire hazards [1]. Effective thermal management is, therefore, essential to keep the battery temperature within the optimal range of 20°C to 40°C.

Furthermore, inconsistent temperature distribution and inadequate heat dissipation within battery packs can adversely affect LIB performance and longevity. Recent developments in battery thermal management systems (BTMSs) have focused on minimizing maximum temperature and enhancing temperature uniformity while reducing cooling energy consumption [2]. BTMSs can be broadly classified into active and passive systems. Active cooling often involves forced convection using air or liquid coolants but can be complex, heavy, and energy-intensive [3]. In contrast, passive methods rely on natural heat transfer mechanisms. Among these, phase change materials (PCMs) have attracted considerable interest due to their high latent heat capacity, which helps regulate battery temperature during high current loads [4]. However, once fully melted, the low thermal conductivity of PCMs can inhibit further effective cooling [5].

Various strategies have been proposed to enhance the thermal conductivity of PCMs, including nanoparticles [6], metallic foams [7], fins [8], wire meshes [9]-[11], and encapsulation techniques [12]. While nanoparticles and fins can improve heat transfer, they may be costly or obstruct natural convection within the melted PCM [6]. Metallic foams and wire meshes can offer a compromise between conductivity enhancement and system weight [7], but achieving optimal porosity is crucial [7]. Partial wire mesh coverage has shown promise, balancing the PCM's latent heat capacity with enhanced conduction [13].

Previous research highlights the effectiveness of wire meshes in improving thermal conductivity without drastically reducing latent heat capacity [9]. Studies employing graphene nanoparticles [6] and metal foams [14] further underscore the importance of combining conductive additives and PCM. Notably, integrating meshes at strategic locations can delay

PCM melting and promote more uniform temperature distribution [10].

In this study, a partial copper wire mesh is embedded within the PCM around high-capacity 21700 cylindrical cells to enhance overall heat dissipation while retaining beneficial convective properties. The focus on partial mesh aims to preserve much of the PCM's latent heat and allow natural convection once melting begins [13]. A comprehensive experimental and analytical framework is developed to measure heat generation, dissipation, and latent energy utilization at varying discharge rates. By investigating mesh placement and performance during the transition from solid to melted PCM, this research provides new insights into optimizing PCM-based battery packs for robust and reliable thermal management.

II. Methodology

A. Experimental Setup

Nine cylindrical lithium-ion batteries (Samsung INR21700-50S, 5000 mAh, nominal voltage of 3.7 V) were arranged in series within a cuboid enclosure fabricated from medium-density fiberboard (MDF), with an internal dimension of 8.4 cm × 8.4 cm × 6.0 cm. Four vertical copper pipes (6 mm outer diameter) were inserted between the cells to facilitate heat dissipation through airflow within the air duct. An air duct measuring 19 mm in height and matching the width of the enclosure was positioned above the battery pack. Airflow was provided by an axial AC fan (GDSTIME 1203) at an inlet speed of 2.1 ± 0.1 m/s. The battery pack was placed inside a thermal chamber (SD-508, Associated Environmental Systems) to simulate an ambient temperature of 22 ± 0.5 °C. An isometric visualization of the battery pack is presented in Fig. 1.

Four layers of square copper wire mesh (#10 mesh number; 1.91 mm opening; 0.64 mm wire diameter; 3.8 cm height) were embedded in a grid configuration around the cells. This mesh occupied 63.5% of the enclosure's height, yielding a porosity of 93% (optimized via [13]). Fig. 2(a) and (b) illustrate the configuration and alignment of the wire mesh in the battery pack.

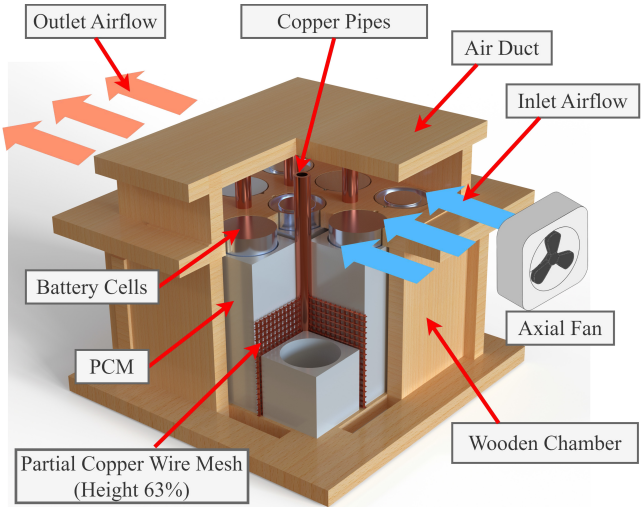

Figure 1. Isometric view of the proposed battery pack.

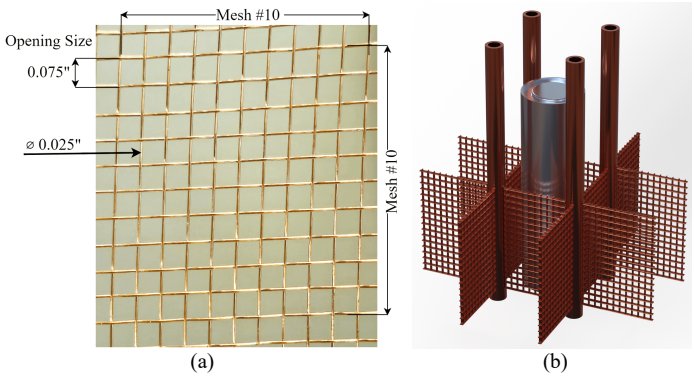

Figure 2. Proposed copper wire mesh: (a) coniguration and (b) grid alignment in the battery pack.

Eight T-type thermocouples (Omega 5TC-TT-T-24-72) were attached to the cells, following the alignment presented in Fig. 3. An additional thermocouple was used to measure the internal temperature of one copper pipe. Temperature data were logged using Adafruit 3263 sensors connected to an Arduino Mega 2560 R3, with a total accuracy of ±0.075 °C. A heat flux sensor (FluxTeq PHFS-01) was also employed to measure the surface heat flux of one cell, providing critical data for assessing heat generation during discharge tests. Heat flux data were recorded using a data acquisition device (NI-9211) with an accuracy of ±0.03 μV/(W/m²).

Paraffin with a melting temperature of 41 ± 1 °C was selected as the PCM due to its high latent heat of fusion and stable performance. In this study, 211 ± 1 mL of molten paraffin (163 ± 1 g) was utilized into the pack, offering a total latent heat capacity of 39.81 kJ. Table I presents the key physical properties of the materials used in this experiment.

B. Experimental Procedure

All experiments have been initially conditioned and performed at a constant ambient temperature of 22 ± 0.5 °C. The nine batteries, connected in series, were charged using a standard 6A two-stage charging protocol (6A constant current followed by 37.8V constant voltage) with a DC power supply (OWON SP6103), featuring an accuracy of ±0.01A and ±0.005V.

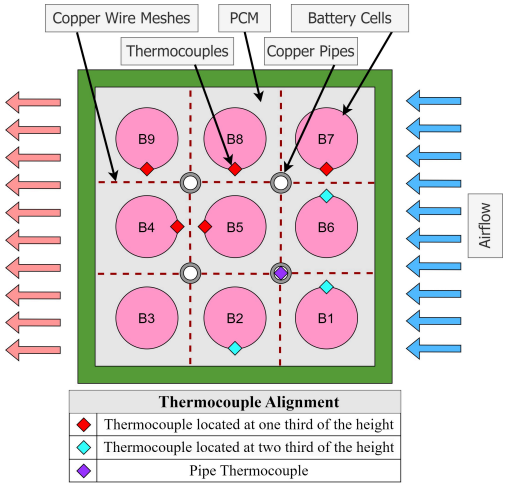

Figure 3. Top view of the battery pack illustrating the layout of the installed thermocouples.

TABLE I. PHYSICAL PROPERTIES OF MATERIALS USED IN EXPERIMENT.

Property	Unit	Copper [11]	Paraffin PCM (solid-liquid) [15]
Specific Heat at Constant Pressure (c_p) [a]	J/kg · K	390	2,150 – 2,250
Thermal Conductivity [a]	W/m · K	401	0.21 – 0.18
Latent Heat (L_f)	kJ/kg	-	245
Liquidus Temperature	°C	-	42
Solidus Temperature	°C	-	39
Electrical Resistivity [a]	$\Omega \cdot m$	1.68×10^{-8} [16]	-

a. The physical properties provided are measured at 25°C and 1 bar.

The discharge process was performed under constant-current loads at discharge rates of 1C, 2C, and 3C, corresponding to 5A, 10A, and 15A, respectively. A multifunctional electronic load (TDI RBL488) with an accuracy of ±0.01A was used for this purpose.

According to the manufacturers' specifications, the cutoff current was defined as 0.01A for both charge and discharge cycles. Fig. 4 illustrates the power usage profiles of the battery pack during discharge at various rates.

C. Heat Transfer Governing Equation

The thermal behavior of the battery pack was governed by the heat balance equation, which equates to the total heat generated (Q_G) to the sum of heat dissipated through the copper pipes (Q_D), sensible energy utilized (Q_S), latent energy utilized (Q_L), and an error term (ε):

$$Q_G = Q_D + Q_S + Q_L + \varepsilon. \quad (1)$$

Q_G was quantified using data from the heat flux sensor, and the total was computed by integrating the heat flux over the entire discharge duration and assuming uniform heat generation in all nine cells.

Q_D through the copper pipes was defined based on convective heat transfer principles. The heat transfer rate was calculated using the convective heat transfer coefficient, which was derived from the Nusselt number under laminar flow conditions. The rate of heat dissipation was expressed as:

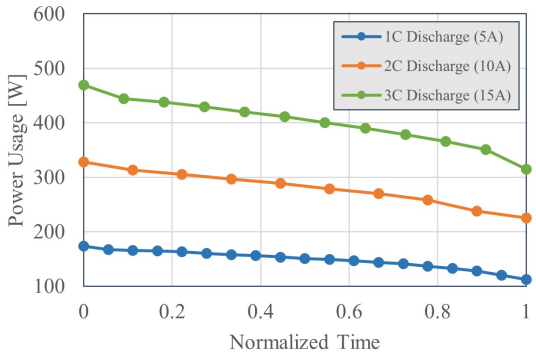

Figure 4. Battery modules discharge power usage.

$$\dot{Q_D} = 4hA_{pipe}(T_{pipe} - T_{inlet}). \quad (2)$$

where h is the convective heat transfer coefficient, A_{pipe} is the effective surface area of the copper pipes in the air duct, and T_{pipe} and T_{inlet} are the temperatures of the pipes and inlet air, respectively. Integrating this equation over the discharge period provided the total heat dissipated.

Sensible heat (Q_S) represents the energy required to raise the temperature of the PCM, excluding the energy required for phase transition. It was calculated using the specific heat capacity of the PCM, the mass of the PCM, and the change in temperature from the initial condition to the final measured state:

$$Q_S = \int C_p(T_f - T_i)dm \approx m_{PCM}C_p(\overline{T_f} - T_i). \quad (3)$$

where $\overline{T_f}$ is the average final temperature recorded by thermocouples, T_i is the initial temperature and C_p is the PCM's specific heat capacity at constant pressure.

The latent heat utilized (Q_L) was determined by subtracting the total heat dissipated (Q_D) and the sensible heat (Q_S) from the total heat generated (Q_G):

$$Q_L = Q_G - (Q_D + Q_S). \quad (4)$$

The maximum available latent heat ($Q_{L,max}$) was calculated based on the PCM mass and its latent heat of fusion, providing a reference for evaluating PCM utilization (39.81 kJ). To assess the effectiveness of the PCM, its melting fraction was determined as the ratio of utilized latent heat to the maximum available latent heat:

$$\beta = {Q_L}/{Q_{L,max}}. \quad (5)$$

This comprehensive energy balance framework enabled a quantitative assessment of the thermal management system's performance, providing insights into how effectively the PCM and copper mesh configuration contributed to regulating battery temperatures under different discharge conditions.

D. Consistency and Uncertainty Analysis

Uncertainty analysis was conducted following Moffat's (1988) methodology [17], distinguishing between bias errors (systematic offsets) and precision errors (random variations in repeated measurements). Bias errors originated from measurement device limitations, with T-type thermocouples (±0.5 °C) and Adafruit sensors (±0.075 °C), resulting in a combined bias error of ±0.51 °C using the root-sum-square (RSS) method. The FluxTeq heat flux sensor had a reported accuracy of ±2 W/m^2 to ±14 W/m^2, varying with discharge rates. Precision errors were assessed by determining the largest deviation from the mean in multiple trials. The maximum observed precision error was ±0.26 °C for temperature and ±10 W/m^2 for heat flux. The total uncertainty was computed by combining relative bias and precision errors through the RSS technique.

Table II summarizes the uncertainty in temperature and heat flux measurements. These values validate the reliability of the experimental setup and confirm the reproducibility of the results.

TABLE II. TOTAL ERROR AND UNCERTAINTY OF THE EXPERIMENTALLY MEASURED PARAMETERS.

Parameter	Reference Value	Relative Bias Error	Max. Relative Precision Error	Max Total Uncertainty
Min. Temperature	20 °C	2.5 %	1.5 %	2.9 %
Max. Temperature	46 °C	1.1 %	0.63 %	1.2 %
Min. Heat Flux	50 W/m^2	4.0 %	3.3 %	5.2 %
Max. Heat Flux	710 W/m^2	2.0 %	1.4 %	2.4 %

III. RESULTS

A. Temperature Analysis

Temperature measurements were taken according to the thermocouple placement presented in Fig. 3. The mean temperature and the maximum temperature difference of the recorded data are illustrated in Fig. 5(a) and Fig. 5(c). As observed, incorporating the copper mesh consistently reduces the maximum temperature. However, at higher discharge rates, slight temperature non-uniformities are introduced across the measured thermocouples. These variations remain negligible, given the small magnitude and the total error margin of the experiments. Fig. 5(b) illustrates the temperature gradient between the pipe temperature and the mean temperature of the cells, which serves as an indicator of the thermal link between the cells and the cooling air duct. A reduction in this gradient signifies enhanced thermal conductivity of the PCM.

At a moderate discharge rate of 1C (5A), the integration of the copper mesh reduced the maximum temperature and temperature gradient by approximately 3.7 ± 0.3 °C and 2.9 ± 0.2 °C, respectively, demonstrating the system's effectiveness in managing heat generation through enhanced conduction.

At discharge rates of 2C and 3C, the mean temperature of the cells reached the melting point of the PCM. Similar to the 1C observations, incorporating the copper mesh effectively enhanced thermal conductivity and reduced the cell temperature while maintaining it within the safe operational limits (2.6 ± 0.3 °C and 4.8 ± 0.3 °C). However, a slight increase in temperature non-uniformity was observed in Fig. 5(c), potentially due to partial utilization of the mesh or its grid configuration around the cells. This increase, approximately 0.6 °C, is within the measurement errors and is considered negligible.

B. Heat Transfer Analysis

The effectiveness of heat dissipation from the battery pack was assessed by comparing the heat dissipation through the copper pipes (Equation (3)) against the total heat generated by the cells (measured via heat flux). The results confirm that the integration of the copper mesh significantly enhances heat transfer, particularly at lower discharge rates. Fig. 6 illustrates the heat dissipation and heat generation profiles for each configuration.

At 1C and 2C, the mesh-PCM configuration facilitated rapid heat dissipation, ensuring that most of the generated heat was efficiently transferred away from the battery cells. Under these conditions, the system reached a near-equilibrium state where heat dissipation closely matched heat generation. This thermal balance is crucial in preventing excessive temperature accumulation and ensuring long-term battery performance.

At 3C, the increased heat generation rate resulted in an imbalance between heat dissipation and heat accumulation. While the system could not reach full thermal equilibrium within the short discharge period, the mesh-enhanced PCM still provided a 20% increase in heat dissipation compared to the pure PCM configuration. This improvement can be attributed to the mesh's role in enhancing the effective thermal conductivity of the PCM, enabling a more efficient heat transfer from the battery cells to the copper pipes and, consequently, to the air duct.

According to heat transfer principles, and assuming that all heat dissipation of the battery pack is primarily through the air duct while the battery pack's walls are thermally insulated, Equation (1) to (3) yield the comparative heat transfer analysis in Fig. 7. This figure presents the total heat generation, total heat dissipation, and utilized sensible energy. Based on Equation (1), the amount of heat generation must balance with the sum of heat dissipation, sensible energy, and the unknown (if necessary) latent energy. Consequently, the remaining amount in the sum of heat dissipation (Q_D) and sensible energy (Q_S) from heat generation (Q_G) must be utilized by the latent energy (Q_L), which in maximum has been calculated to be 39.81 kJ due to the mass and latent heat of the PCM.

At discharge rates of 1C and 2C, the mesh-enhanced PCM provides sufficient heat dissipation to meet the total heat generation without relying on latent energy. In contrast, in the pure PCM system, even at 1C (5A) discharge, the latent heat becomes necessary to handle the generated heat. As the discharge rate surpasses 2C, the experiment duration shortens, and the heat generation rate spikes, causing the amount of dissipation and sensible energy to be insufficient to reach heat generation, thereby necessitating PCM melting. Moreover, for all tested discharge rates, the amount of heat dissipation remains approximately constant at 10 kJ and 15 kJ for pure PCM and mesh-PCM configurations, respectively. The integration of the mesh within the PCM consistently demonstrated a 20-40% increase in heat dissipation.

Overall, the analysis of Fig. (7) underscores the notable roles of discharge rates in governing the battery pack performance. The system performs effectively at lower ambient discharge rates (1C and 2C), where sufficient heat dissipation is achieved by utilizing the mesh within the PCM.

C. PCM Latent Heat Utilization Analysis

The reliance on PCM latent heat was evaluated by analyzing the heat balance equation, comparing the energy stored as sensible heat and dissipated through the copper pipes to the total heat generated. The difference represents the latent heat contribution, further expressed as the PCM melting fraction by dividing it by the maximum latent energy ($Q_{L,max}$). Table III summarizes the PCM melting fraction across all tested discharge rates.

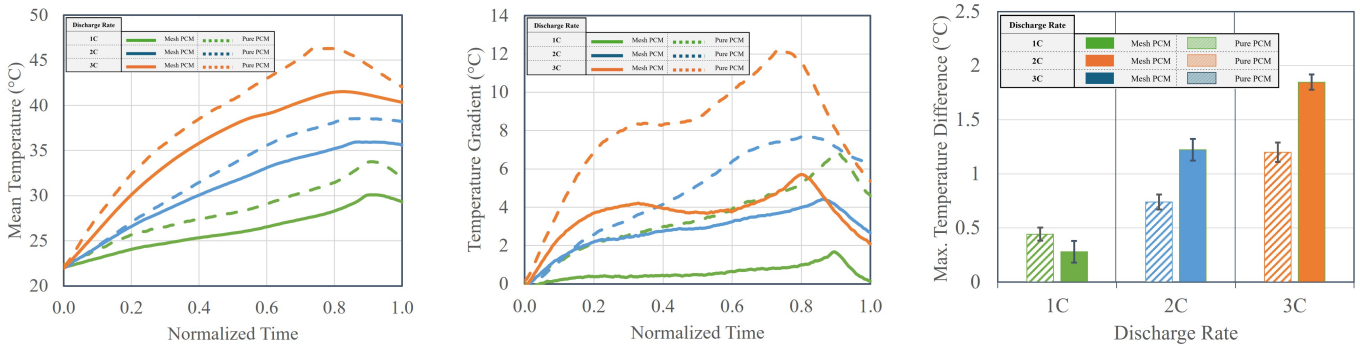

(a) (b) (c)

Figure 5. Temperature analysis of cases with and without mesh, including (a) mean temperature, (b) temperature gradient, and (c) maximum temperature difference.

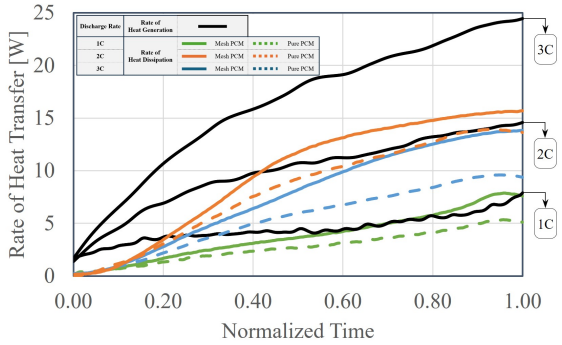

Figure 6. Rate of heat transfer within the proposed battery pack, indicating heat generation and dissipation rates at various discharge rates.

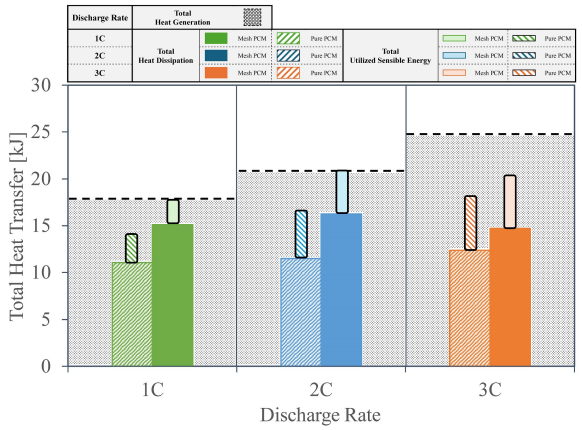

Figure 7. Total heat transfer within the proposed battery pack, indicating heat generation, dissipation, and sensible energy at various discharge rates.

TABLE III. PCM LATENT ENERGY UTILIZATION PERCENTAGE (MELTING FRACTION) ACROSS VARIOUS DISCHARGE RATES.

PCM Configuration	Discharge rate		
	1C	2C	3C
Pure PCM	8.5 %	9.8 %	15.3 %
Mesh-PCM	0.0 %	0.0 %	9.9 %

At discharge rates of 1C and 2C, the mesh-PCM configuration exhibited optimized thermal performance, effectively managing heat without requiring significant latent heat utilization. Heat dissipation and sensible heat storage alone regulated battery temperatures, resulting in a 0% PCM melting fraction for the mesh-enhanced setup. This indicates that under moderate thermal loads, copper mesh integration significantly reduces dependence on phase change mechanisms, preserving PCM's latent capacity for higher stress conditions.

At 3C, latent heat utilization became necessary to accommodate excess heat that could not be dissipated through conduction and sensible heat absorption alone. However, the mesh-PCM system exhibited a lower melting fraction (9.9%) than the pure PCM setup (15.3%). This reduction underscores the role of the copper mesh in delaying PCM melting, enhancing heat dissipation efficiency, and improving the system's operational stability.

IV. CONCLUSIONS

This study experimentally investigated the thermal performance of a PCM-based battery pack enhanced with copper mesh. Nine series-connected 21700 cells (5000 mAh) were subjected to three constant current discharge rates of 1C to 3C under the constant ambient temperature of 22 °C. The analyses quantified heat generation, heat dissipation, sensible energy, and latent heat utilization of the PCM. The novelty of this work lies in incorporating a partial copper wire mesh directly within the PCM-based battery pack and experimentally assessing its performance based on heat dissipation and PCM melting fraction. The results demonstrated that incorporating copper mesh significantly improved heat dissipation, reduced reliance on latent heat utilization, and enhanced battery temperature regulation under various discharge rates. Key findings include:

- The mesh-PCM configuration reduced the maximum temperatures by 3.7, 2.6, and 4.8 °C during 1C to 3C discharge rates, respectively.
- The mesh-PCM configuration increased heat dissipation by 20-40% compared to the pure-PCM case.

- At lower discharge rates (1C and 2C), the incorporation of copper mesh enabled sufficient heat dissipation and sensible heat storage to regulate battery temperature effectively, eliminating the need for latent heat utilization. Conversely, in the pure-PCM configuration, the PCM melting fraction was determined to be 8.5% and 9.8% at 1C and 2C, respectively.
- At a high discharge rate (3C), the mesh-PCM configuration reduced the PCM melting fraction from 15.3% (pure PCM) to 9.9%, demonstrating improved thermal efficiency and a delayed phase transition.

These findings suggest that integrating copper mesh into PCM-based battery thermal management systems significantly enhances cooling performance, particularly in applications requiring sustained high-power operation. By effectively reducing peak temperatures and minimizing reliance on latent heat storage, this approach offers a streamlined yet highly efficient alternative to conventional cooling methods. Future research should focus on optimizing mesh parameters–such as placement, porosity, height distribution, and material composition–to further improve heat dissipation and ensure reliable performance under higher discharge rates.

ACKNOWLEDGMENT

The authors acknowledge with gratitude the financial support provided by the Natural Sciences and Engineering Research Council of Canada (especially the NSERC CREATE and NSERC Discovery Grant programs).

NOMENCLATURE

C	Discharge rate (1/hour)
C_p	Specific heat at constant pressure (kJ/kg.K)
h	Convective heat transfer coefficient (W/m²·K)
L_f	PCM's latent heat of fusion (kJ/kg)
m_{PCM}	Total mass of the PCM (kg)
$\dot{Q}$	Rate of heat transfer (W)
Q	Total heat transfer (J)
T	Temperature (°C)

GREEK SYMBOLS

β	PCM melting fraction (%)
ε	Error term in heat transfer (W)

ABBREVIATIONS AND ACRONYMS

BTMS	Battery Thermal Management System
LIB	Lithium-Ion Battery
MDF	Medium-Density Fiberboard
NSERC	Natural Sciences and Engineering Research Council of Canada
PCM	Phase Change Material

REFERENCES

[1] Luo, J., Zou, D., Wang, Y., Wang, S., & Huang, L. (2022). Battery thermal management systems (BTMs) based on phase change material (PCM): A comprehensive review. *Chemical Engineering Journal*, 430, 132741.

[2] Wang, M., Teng, S., Xi, H., & Li, Y. (2021). Cooling performance optimization of air-cooled battery thermal management system. *Applied Thermal Engineering,* 195, 117242.

[3] Huang, M., Eames, P., Norton, B., & Hewitt, N. (2011). Natural convection in an internally finned phase change material heat sink for the thermal management of photovoltaics. *Solar Energy Materials and Solar Cells*, 95, 1598-1603.

[4] Ganji, M. J., Agelin-Chaab, M., & Rosen, M. A. (2025). Experimental investigation on incorporating wire mesh into a PCM-based battery pack in elevated ambient temperatures. Unpublished.

[5] Ganji, M. J., Agelin-Chaab, M., & Rosen, M. A. (2025). Experimental Investigation of Phase Change Material-Based Battery Pack Performance Under Elevated Ambient Temperature. *Batteries*, 11(2), 67.

[6] Kadam, G., & Kongi, P. (2023). Battery thermal management system based on PCM with addition of nanoparticles. *Materials Today: Proceedings*, 72, 1543-1549.

[7] Ranjbaran, Y. S., Haghparast, S. J., Shojaeefard, M. H., & Molaeimanesh, G. R. (2020). Numerical evaluation of a thermal management system consisting PCM and porous metal foam for Li-ion batteries. *Journal of Thermal Analysis and Calorimetry*, *141*, 1717-1739.

[8] Ping, P., Peng, R., Kong, D., Chen, G., & Wen, J. (2018). Investigation on thermal management performance of PCM-fin structure for Li-ion battery module in high-temperature environment. *Energy Conversion and Management*, *176*, 131-146.

[9] Situ, W., Zhang, G., Li, X., Yang, X., Wei, C., Rao, M., Wang, C., Wu, W. (2017). A thermal management system for rectangular $LiFePO_4$ battery module using novel double copper mesh-enhanced phase change material plates. *Energy*, *141*, 613-623.

[10] Wu, W., Yang, X., Zhang, G., Ke, X., Wang, Z., Situ, W., Li, X., Zhang, J. (2016). An experimental study of thermal management system using copper mesh-enhanced composite phase change materials for power battery pack. *Energy*, *113*, 909-916.

[11] Ebadi, S., Tasnim, S. H., Aliabadi, A. A., & Mahmud, S. (2020). An experimental investigation of the charging process of thermal energy storage system filled with PCM and metal wire mesh. *Applied Thermal Engineering*, *174*, 115266.

[12] Safdari, M., Ahmadi, R., & Sadeghzadeh, S. (2020). Numerical investigation on PCM encapsulation shape used in the passive-active battery thermal management. *Energy*, *193*, 116840.

[13] Ganji, M., Givian, M., Gharali, K., Ebadi, S., & Dastjerdi, S. M. (2023). Experimental optimization of partial metallic wire mesh configuration applicable in thermal energy storage systems. *Applied Thermal Engineering*, 218, 119274.

[14] Isfahani, M. S., Gharehghani, A., Saeedipour, S., & Rabiei, M. (2023). PCM/metal foam and microchannels hybrid thermal management system for cooling of Li-ion battery. *Journal of Energy Storage*, *72*, 108789.

[15] LeePeng, P., Wang, Y., & Jiang, F. (2022). Numerical study of PCM thermal behavior of a novel PCM-heat pipe combined system for Li-ion battery thermal management. *Applied Thermal Engineering*, 209, 118293.

[16] Halliday, D., Resnick, R., & Walker, J. (2021). *Fundamentals of physics* (12th ed.). John Wiley & Sons.

[17] Moffat, R. J. (1988). Describing the uncertainties in experimental results. *Experimental thermal and fluid science*, 1(1), 3-17.